ACS APPLIED ENERGY MATERIALS

www.acsaem.org Article

# Quasi-2D Carrier Transport in KMgBi for Promising Thermoelectric Performance

Vikram,[§] Bhawna Sahni,[§] Ankit Jain, and Aftab Alam*

Cite This: *ACS Appl. Energy Mater.* 2022, 5, 9141−9148 Read Online

ACCESS | Metrics & More | Article Recommendations | Supporting Information

**ABSTRACT:** KMgBi is an interesting system with several unconventional electronic transport properties. Despite numerous studies exploring its topological trivial/nontrivial nature, it has never been studied from a thermoelectric (TE) perspective. Its band structure shows appropriate degenerate flat bands near the valence band edge that are useful for high thermopower. We also show that KMgBi acquires a high degree of anharmonicity that leads to low lattice thermal conductivity. This yields a high TE figure of merit, $ZT \sim 2.21$ (p-type) at ∼600 K temperature. A careful analysis of electron and phonon dispersion establishes an interesting quasi-2D nature of KMgBi. Utilizing the flat degenerate valence band and strong spin−orbit coupling, we discuss how to further enhance the TE performance of KMgBi via alloy engineering. Substituting Li at K and As at Bi sites increases the band gap with little effect on the band curvature, further improving the TE performance. With 50% As alloying, we expect ∼10−11% enhancement in the $ZT$.

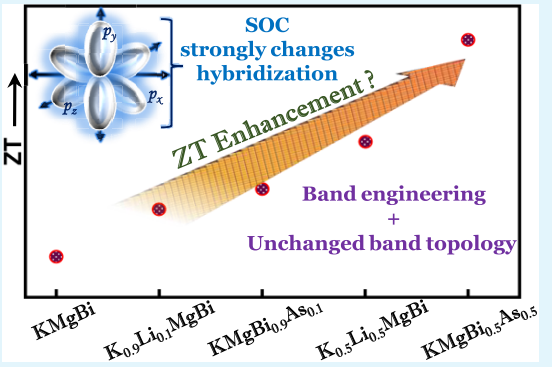


**KEYWORDS:** *energy material, quasi-2D material, thermoelectrics, electronic structure, relaxation time, electronic transport, phonon transport*



## INTRODUCTION

The ever-increasing demand of energy requires a concentrated effort to broaden our renewable energy resources. A large fraction of energy consumed around us is often lost as waste heat. Conversion of such heat into other forms of usable energy can significantly impact the global energy requirement. Over the past few years, thermoelectrics has emerged as an important research field that converts such waste heat into electricity. In the quest for finding novel materials to meet/enhance the thermoelectric (TE) conversion efficiency, several classes of compounds have been explored in the past decades.[1−9,11,12] Among these, ternary half-Heusler alloys (HHAs) have emerged as promising candidates for TE applications because of their reasonable band gap values, high Seebeck coefficient, and appealing transport properties. Interestingly, HHAs have the potential to replace some of the state of the art TE materials.[13−16] In the recent past, there has been extensive effort to find new HHAs with promising TE properties. One of the best HHAs found so far is the family of ANiSn (A = Ti, Zr, or Hf)-related compounds with maximum reported $ZT$ values ranging between 0.7 and 1.3.[10−12] Apart from these, NbCoSn ($ZT \sim 0.15$),[17] TiCoSb ($ZT \sim 0.015$),[18] and others have emerged as promising HHA candidates. All these compounds belong to the 18-valence-electron HH family. Similar efforts to discover new materials also lead to an extensive investigation of the eight-electron HH family.[19−23] In pure HHAs (without doping), the TE figure of merit turns out to be relatively small because of the small magnitude of power factor and large thermal conductivity. Thus, it is important to tune the governing parameters in any pure (ideal) crystal via doping/pressure to improve their TE performance. The effect of doping in ideal crystals can be theoretically studied using the semiclassical Boltzmann transport equation. Thus, simulations can guide us in making an educated guess and reducing the resources/time toward experimental realization of promising TE materials. In this article, we discuss an important ternary half-Heusler compound, KMgBi.

KMgBi has been discussed in various density functional theory (DFT)-based studies in the cubic,[24,25] hexagonal,[26] and tetragonal[27,28] phases for optoelectronics, ferroelectrics, and topological insulator applications, respectively. Experimentally, it has been reported to crystallize in the tetragonal phase ($P4/nmm$, no. 129) at room temperature.[29] Theoretically, this tetragonal phase of KMgBi is predicted to show a band gap ($E_g$) of 363 meV within generalized gradient approximation (GGA), which closes when spin−orbit coupling (SOC) effects

Received: June 1, 2022
Accepted: June 28, 2022
Published: July 14, 2022

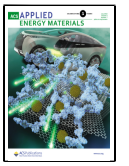

are included.[27] This SOC-driven band gap closure and the observed band inversion predict KMgBi to be a candidate as a topological Dirac semimetal (DSM). The experimental study by Zhang et al.,[29] however, confirms KMgBi to be a narrow band gap semiconductor with $E_g \sim 11.2$ meV. Taking insights from these experimental findings, Le et al.[27] used a more accurate HSE03 functional to reproduce the experimental band gap and showed that even though KMgBi is topologically trivial, the DSM phase can be achieved with external strain or doping of the K-site with isovalent heavier elements (Rb, Cs). In addition to the conflicting trivial/nontrivial nature of the electronic band structure, an interesting feature of KMgBi is the presence of the degenerate flat bands at/near the valence band edge.[27] Such feature is not paid too much attention in the literature, but this feature can facilitate very high density of states at/near the Fermi level ($E_F$) and is highly preferred for TE applications.

Despite various reports, KMgBi has never been explored from a thermoelectric perspective. In this article, we first confirm KMgBi to show a quasi-2D nature. The quasi-2D materials display unique electronic, optical, and thermal properties and thus can be potential candidates for thermal management and energy conversion, electronics, etc.[30,31] The distinct properties of such layered cystal structures, like KMgBi, are dictated by the bonding strength between inter- and intra-layers and are thus interesting to analyze. Additionally, these materials exhibit reasonably low lattice thermal conductivity[32] and hence are extremely useful for high TE performance. With this background, we present a detailed report confirming KMgBi to be a promising candidate for TE applications whose efficiency can further be enhanced with suitable alloy engineering. Our results are based on the calculation of highly accurate band gaps/order using the HSE06+GW scheme including the SOC effect. This is then followed by the explicit evaluation of thermoelectric properties. Most importantly, we made a careful attempt to accurately calculate the lattice thermal conductivity ($\kappa_L$) and the carrier relaxation time ($\tau$), which is required for a reliable estimate of the TE figure of merit ($ZT$). Detailed insight into the contribution of optical phonon modes to the lattice thermal conductivity and its effect on $ZT$ is also presented. Intrigued by the interesting flat valence band feature as a consequence of the quasi-2D nature and strong SOC effects in KMgBi, we have further explored the possibility of improving its TE performance via alloy engineering.

## COMPUTATIONAL/THEORETICAL DETAILS

We employ first-principles *ab initio* simulations within DFT[33] as implemented in the Vienna *Ab initio* Simulation Package (VASP)[34−36] with a projector augmented-wave basis[37] and the GGA exchange-correlation functional of Perdew−Burke−Ernzerhof (PBE).[38] For more reliable estimates of band gap and band order, hybrid HSE06[39] and HSE06+GW[40] schemes are used. The effect of spin−orbit coupling is included explicitly in the calculations. A plane wave energy cutoff of 500 eV and a Brillouin zone (BZ) sampling using Γ-centered *k*-mesh is done for all the calculations. Different *k*-point meshes are used at different levels of calculations, details of which are provided in the Supporting Information.[41] Cell volume, shape, and atomic positions for all the structures are fully relaxed using a conjugate gradient algorithm until the energy (force) on each atom converge below $10^{-6}$ eV (0.001 eV/Å).

At a given absolute temperature, $T$, the conversion efficiency of a TE device depends upon the transport coefficients of the constituent material through the following dimensionless figure of merit ($ZT$),

$$ZT = \frac{S^2\sigma}{(\kappa_e + \kappa_L + \kappa_b)}T \quad (1)$$

where $S$ is the Seebeck coefficient, $\sigma$ is the electrical conductivity, and $\kappa_e$ and $\kappa_L$ are the thermal conductivity with respect to electrons and phonons, respectively. It is always a major challenge to enhance $ZT$ as the transport parameters $S$, $\sigma$, and $\kappa$ ($\kappa_e$ and $\kappa_L$) are inter-related and primarily depend upon the electron/phonon dispersion, carrier concentration, and other system-dependent properties. $\kappa_b$ is the bipolar component to the thermal conductivity. Further details explaining these components are provided in the Supporting Information.[41]

*Ab Initio* Scattering and Transport (AMSET)[42] code was used to calculate electronic transport properties; it uses the energy- and temperature-dependent carrier relaxation time to evaluate the transport distribution function while solving the Boltzmann transport equations. The lattice thermal conductivity $\kappa_L$ was calculated, including both three-phonon and four-phonon scattering. Both in-plane and out-of-plane contributions are explicitly shown. Further calculation details are given in the Supporting Information.[41]

## RESULTS AND DISCUSSION

**Electronic Structure.** KMgBi is experimentally reported to crystallize in a tetragonal structure (space group *P*4/*nmm* (no. 129))[29] with Mg−Bi and K atomic layers stacked above each other along the *c* axis, as shown in Figure 1a. The reciprocal

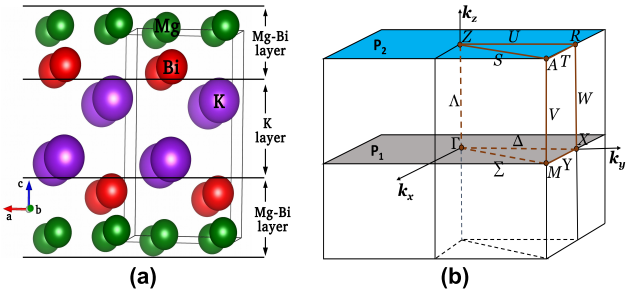


**Figure 1.** (a) Tetragonal crystal structure (space group *P*4/*nmm*, no. 129) of KMgBi showing the stacking of K and Mg−Bi layers. The box sketched by solid lines indicates the unit cell. (b) The reciprocal lattice unit cell of KMgBi showing the high-symmetry *k*-points.

lattice unit cell along with the high-symmetry *k*-points are shown in Figure 1b. The theoretically optimized lattice constant is found to be $a$ = 4.94 Å and $c$ = 8.55 Å, which are in excellent agreement with previously reported theoretical values of $a$ = 4.93 Å and $c$ = 8.54 Å.[27] The reported experimental values for the same are $a$ = 4.88 Å and $c$ = 8.37 Å.[29] Using the PBE exchange-correlation functional, we found KMgBi to be semiconducting with a band gap of 0.35 eV, which agrees well with a reported theoretical value of 0.36 eV.[27] Because Bi is a heavy element, it is important to take into account the effect of SOC. Theoretically, SOC has been reported to close the band gap, giving rise to the 3D Dirac semimetallic phase.[27] However, experimental findings reveal that it indeed has a very small band gap of ∼11.2 meV,[29] with


https://doi.org/10.1021/acsaem.2c01685
ACS Appl. Energy Mater. 2022, 5, 9141−9148

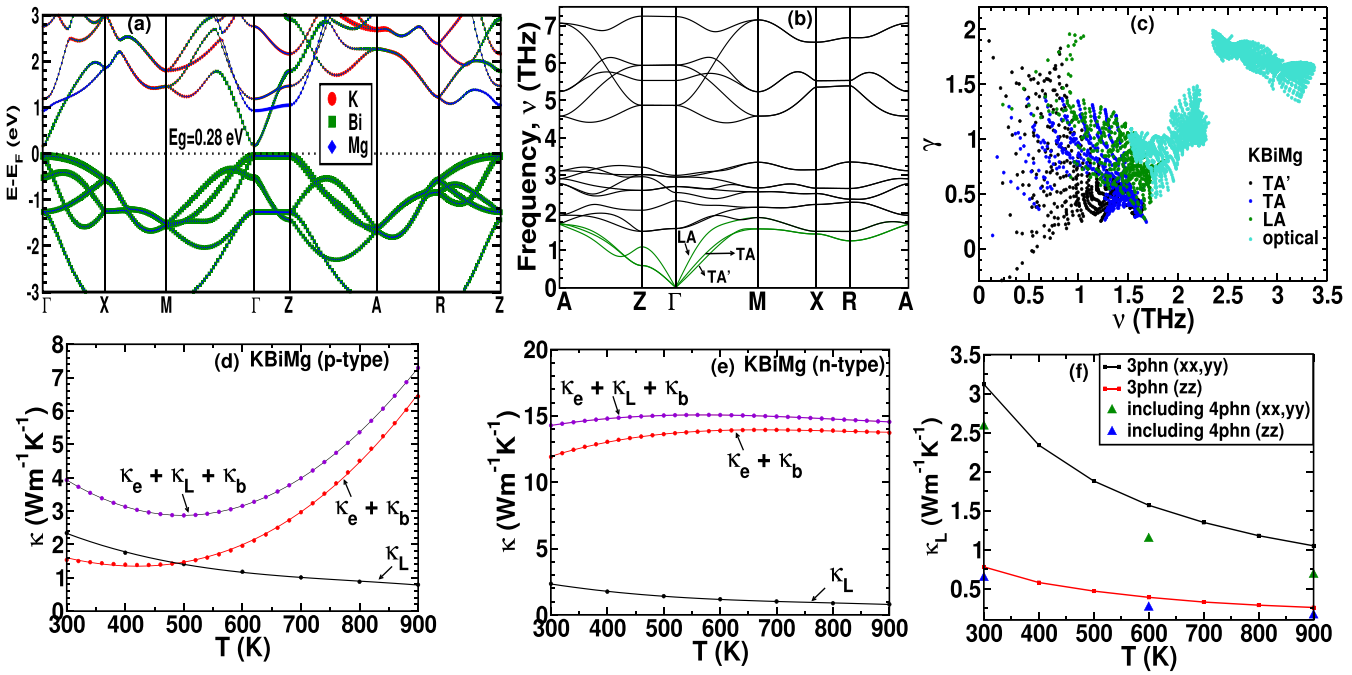


**Figure 2.** For pure KMgBi, (a) the atom projected band structure along the high-symmetry lines of BZ where the band gap is scaled to the value obtained from HSE06+GW+SOC calculations, (b) the phonon band structure, (c) the mode gruneisen parameter ($\gamma$), (d, e) electronic ($\kappa_e + \kappa_b$) and lattice ($\kappa_L$) components of the thermal conductivity ($\kappa$) (three-phonon scattering) for p-type and n-type conductions calculated at carrier concentrations of $1 \times 10^{20}$ and $4 \times 10^{18}$ $cm^{-3}$, respectively, and (f) lattice thermal conductivity values ($\kappa_L$) calculated by including three-phonon and four-phonon scattering processes.

topological nontrivial band ordering. This discrepancy calls for a closer inspection of the electronic band structure with a more accurate hybrid functional (HSE06) including the SOC effects.

The electronic band structure of KMgBi using PBE and HSE06 functionals, with and without SOC, is shown in Figure SI of the Supporting Information.[41] Note that, at the PBE level, the nature of the band gap is direct ($E_g$ = 0.35 eV), but with the inclusion of SOC, the gap closes. The nature of bonding and effect of inclusion of SOC is explained in section II of the Supporting Information.[41] At the HSE06 level, the band gap increases to 0.83 eV, keeping the band curvature almost the same. Interestingly, when SOC effects are included within the HSE06 functional, the gap value decreases, but unlike the PBE case, a small band gap ($E_g$ = 0.22 eV) still persists. This is very similar to the findings of Le et al.,[27] who despite claiming KMgBi to be a 3D Dirac semimetal, showed that HSE03+SOC can open up a gap if the amount of exact Hartree−Fock exchange is tuned via the mixing parameter $\alpha$. To avoid the dependence on any mixing parameter, we performed the linear response GW+SOC calculation within the hybrid (HSE06) functional, which is fully *ab initio* in nature and is known to give the theoretically most accurate estimate of the band gap.[43] A band gap of 0.28 eV thus obtained is the best theoretical prediction for KMgBi ever reported in the literature, which will be used for our additional TE simulation. Our present findings are also consistent with the experimental work of Zhang et al.,[29] which reported KMgBi to be a small band gap material.

Figure 2a shows the atom projected band structure of KMgBi within the PBE functional with its band gap scaled to the value obtained from HSE06+GW+SOC calculations. This is reasonably acceptable for two reasons: (i) no noticeable changes in the band curvature obtained from the PBE versus HSE06 functional except the magnitude of the band gap (see Figure SI of the Supporting Information[41]). (ii) HSE06-SOC calculations are computationally an order of magnitude more expensive than PBE+SOC calculations. The valence band edges mostly acquire Bi and Mg characteristics, whereas the conduction band edges are dominantly contributed by K atoms. The conduction band edges have some contributions from the other two atoms as well. The occupied bands along the Γ−*M* or Γ−*X* direction are dispersive, in contrast to bands along the Γ−*Z* direction, which suggests that the thermoelectric properties vary in in-plane and out-of-plane directions. The very flat nature of valence bands along the Γ−*Z* direction (from the BZ center toward the boundary) indicates a quasi two-dimensional (2D) behavior of KMgBi toward the hole transport. Interestingly, the occupied bands are symmetric along the two planes P1 (Γ−*M*−*X*) and P2 (*Z*−*A*−*R*), as shown in Figure 1b). This points toward a similar type of hole transport in the two planes P1 and P2, further strengthening our idea of a quasi-2D structure for hole transport. The most interesting feature is the occurrence of flat bands along the Γ−*Z* direction, which leads to a very high effective mass. This suggests that KMgBi can be a very good p-type TE material with high thermopower.

**Phonon Properties.** Figure 2b shows the phonon dispersion of pure KMgBi. The primitive unit cell has six atoms, giving rise to a total of 18 phonon branches. The acoustic and optical modes of vibration are shown by green and black lines, respectively. The phonon density of states (DOS) and the effect of LO-TO splitting on the phonon band structure are shown in section III of the Supporting Information.[41] When one looks at the phonon DOS in Figure SVIII(b) of the Supporting Information,[41] it is clear that the major contributions to the low-energy modes arise from Bi and K atomic vibrations, whereas the Mg vibrations are separated



https://doi.org/10.1021/acsaem.2c01685
ACS Appl. Energy Mater. 2022, 5, 9141−9148

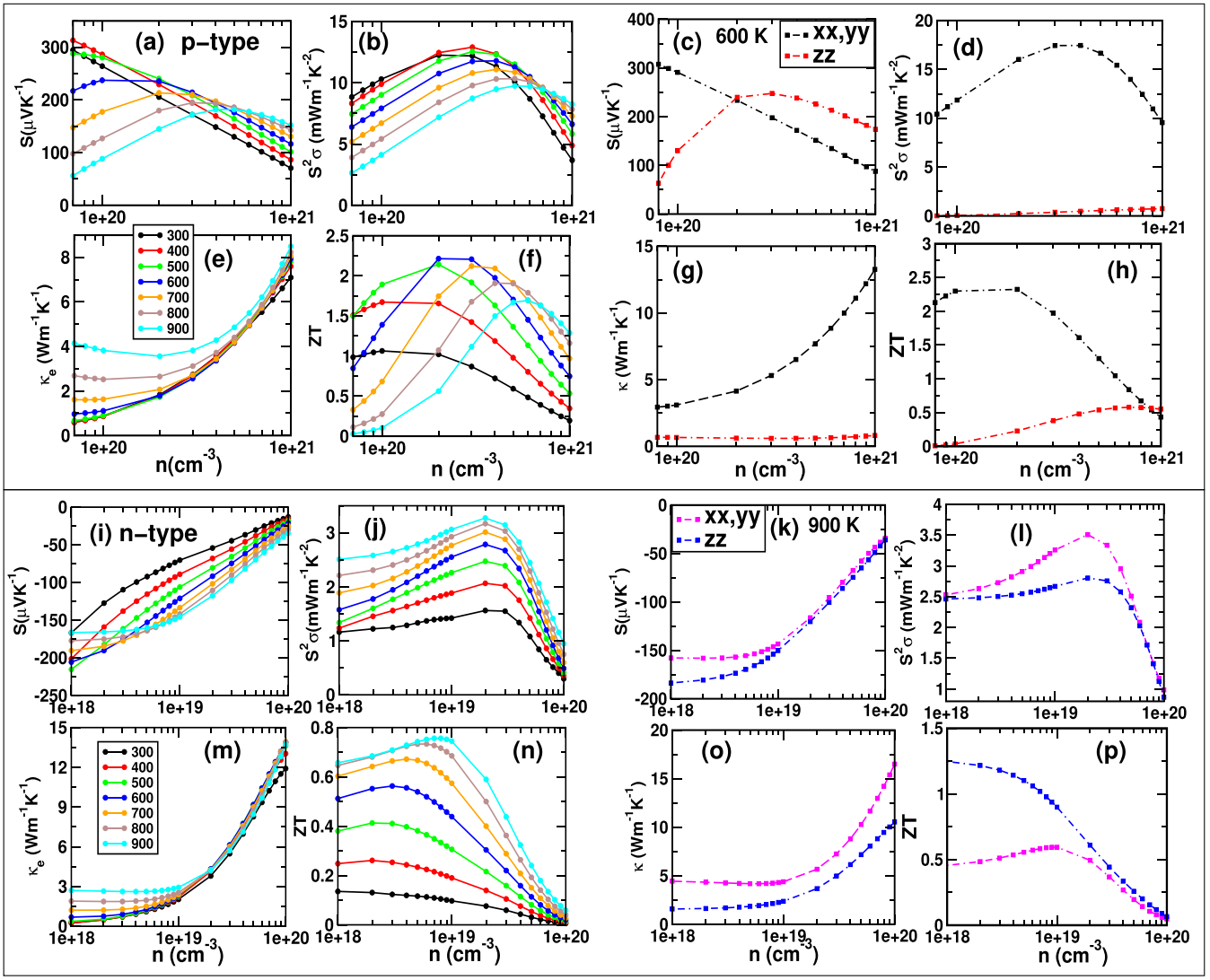


**Figure 3.** For KMgBi, the carrier concentration ($n$) dependence of the Seebeck coefficient ($S$), power factor ($S^2\sigma$), electronic thermal conductivity ($\kappa_e$), and TE figure of merit ($ZT$) at different temperatures ($T$) in the upper left panel (a,b,e,f) for p-type conduction and in the lower left panel (i,j,m,n) for n-type conduction, respectively. The right column shows the anisotropy in the Seebeck coefficient ($S$), power factor ($S^2\sigma$), total thermal conductivity ($\kappa$), and $ZT$ versus $n$ at the temperatures corresponding to the maximum $ZT$ values for (c,d,g,h) p-type (600 K) and (k,l,o,p) n-type (900 K) conductions, respectively.

by a frequency gap in the phonon dispersion. This indirectly reconfirms the quasi-2D nature of KMgBi, reflected in the phonon transport as well. One can see the mixing of low-energy optical phonon modes with the acoustic phonon branches, which are often responsible for the reduction of lattice thermal conductivity due to additional scattering. The higher optical modes (above the gap region) show perfect symmetry and a similar nature along the two planes P1 and P2 of the BZ (see Figure 1b). Additionally, the bands along the direction of high-symmetry points from P1 to P2 ($\Gamma-Z$ and $X-R$) are almost flat, again confirming the quasi-2D nature of KMgBi toward the phonon transport. As evident from Figure 2b, the two TA and TA′ bands are degenerate along $\Gamma$ to $Z$, but they split along the $\Gamma$ to $M$ direction. Figure 2c shows the frequency dependence of $\gamma$, which accounts for the change in phonon mode frequencies with small changes in the volume. In other words, $\gamma$ is a measure of the degree of anharmonicity of the lattice; the higher the $\gamma$-value, the more anharmonic the lattice, resulting in additional scattering that leads to the reduction of $\kappa_L$. The gruneisen parameters ($\gamma_{LA}$, $\gamma_{TA}$, and $\gamma_{TA'}$) for each LA, TA, and TA′ mode and the overall average gruneisen parameter ($\gamma$) of a given system can be obtained from the $\gamma$ versus frequency plot (Figure 2c). In the present case, the $\gamma$-values for all three acoustic branches are quite high. This indicates a higher degree of anharmonicity in KMgBi and hence low $\kappa_L$. The phonon thermal conductivity, in the $\alpha$-direction, $k_\alpha$, is obtained using the Boltzmann transport equation and Fourier's law, as[44,45]

$$k_\alpha = \sum_\lambda c_\lambda {v_{\lambda,\alpha}}^2 \tau_{\lambda,\alpha} \tag{2}$$

where the summation is over all the phonon wave vectors, $\mathbf{q}$, and polarizations, $\nu$, enumerated by composite index $\lambda = (\mathbf{q},\nu)$. $c_\lambda$ is the phonon specific heat, $v_{\lambda,\alpha}$ is the $\alpha$ component of the phonon group velocity vector $\mathbf{v}_\lambda$, and $\tau_{\lambda,\alpha}$ is the phonon scattering time. Theoretical details regarding the computation of $c_\lambda$, $v_{\lambda,\alpha}$, and $\tau_{\lambda,\alpha}$ are available in ref 46. The phonon scattering rates are obtained by considering the three-phonon and four-


https://doi.org/10.1021/acsaem.2c01685
ACS Appl. Energy Mater. 2022, 5, 9141−9148

phonon scattering processes, the details about which can be found in ref 46. Figure 2f shows the lattice thermal conductivity versus the temperature calculated by including three-phonon scattering only and then by including four-phonon scattering as well (at 300, 600, and 900 K). Clearly, the four-phonon scattering causes a reduction in the lattice thermal conductivity as compared to three-phonon scattering. Interestingly, the overall contributions from four-phonon scattering is not much. Thus, we have now calculated the $ZT$ values using the lattice thermal conductivity data obtained from three-phonon scattering processes. For more details about the calculation of $\kappa_L$, please see section I of the Supporting Information.[41] $T$-Dependence of the calculated $\kappa_L$ is shown in Figure 2d,e.

**Thermoelectric Properties.** Most theoretical simulations of TE properties are based on constant relaxation time approximation (CRTA).[47,48] However, the solution of Boltzmann transport equations[49] under CRTA is grossly incorrect because of the complex nature of scattering, leading to the energy- and temperature-dependent carrier relaxation time. This eventually results in an incorrect estimation of the electronic transport properties ($S$, $\sigma$, and $\kappa_e + \kappa_b$). Recently, an *ab initio* approach has been proposed by Ganose et al.[42] to calculate the energy- and temperature-dependent carrier scattering rates, which includes the full anisotropic nature of the acoustic deformation potential (ADP), polar optical phonon (POP), piezoelectric (PIE), and ionized impurity (IMP) scattering processes and has been shown to predict the electronic transport properties with decent accuracy. The ADP, POP, and IMP scattering rates as a function of carrier concentration at different temperatures is shown in the Supporting Information. The PIE scattering rate is neglected because the piezoelectric tensor values were 0. With an increase in carrier concentration, the charge carriers near the ion cores effectively shield the outer carriers from scattering, which affects the scattering mechanisms involving the effective ionic charge (POP and IMP scattering). Thus, the effective carrier screening is taken into account within the limits of AMSET code. The $ZT$ values obtained without carrier screening effects is shown in Figure SXVII of the Supporting Information for comparison. The variation of total carrier relaxation time ranges for electrons and for holes, in the temperature range 100−900 K, is shown in Figure SXVI of the Supporting Information.[41] These relaxation times were then used to calculate the electronic transport properties within the AMSET code.

The lattice thermal conductivity plays a crucial role in the accurate prediction of the thermoelectric figure of merit. Interestingly, the lattice thermal conductivity values are low for the reasons explained earlier. Figure 2d,e shows various components of thermal conductivity [($\kappa_e + \kappa_b$) together and $\kappa_L$] (where $\kappa_L$ is obtained from calculating phonon scatttering rates from three-phonon scattering processes) for p-type and n-type KMgBi, respectively. Figure 3 shows various thermoelectric properties (Seebeck coefficient $S$, power factor $S^2\sigma$, and TE figure of merit $ZT$) and electronic thermal conductivity($\kappa_e$) as a function of carrier concentration ($n$). The change in carrier concentration arises from the varying chemical potential that can be thought of as mimicking the effect of doping/alloying in the host material, as long as the shape of the band structure and the band gap does not alter much with doping/alloying (the so-called rigid band approximation).

It is important to note that, for intrinsic semiconductors, the minority charge carriers come into play when the temperature is sufficiently high to cause the generation of electron−hole pairs and the excitation of electrons across the band gap. The contribution to thermal conductivity due to such a process is called the bipolar thermal conductivity ($\kappa_b$).[50] For heavily doped semiconductors, the effect of $\kappa_b$ can be neglected because the relative carrier concentration generated due to such thermal agitation is very low compared to the number of carriers induced by the dopants. Thus, the effect of bipolar conduction only becomes relevant at lower carrier concentrations and increases with temperature. In the case of KMgBi, the small band gap ($E_g$ = 0.28 eV) does not require much thermal energy to create the electron−hole pair, and hence it excites the generated electrons in the conduction bands. The effect of bipolar conduction is evident from the variation of the Seebeck coefficient and the electronic thermal conductivity, $\kappa_e$ (see Figure 3) at relatively lower carrier concentration. As obvious from the figure, the Seebeck coefficients are significantly suppressed in the low carrier concentration region for both n- and p-type conduction when the temperature is increased from 300 to 900 K. On the other hand, electronic thermal conductivity at lower carrier concentrations and higher temperatures is more due to bipolar contribution.

The peak value of the figure of merit ($ZT_{max}$) for p- and n-type conduction usually occurs at different doping levels for p-type and n-type carriers. This is due to the different natures of bands and scattering. While showing various components of the thermal conductivity (in Figure 2d,e), we have chosen those doping concentrations for the two carriers at which the figure of merit ($ZT$) is maximum (= $ZT_{max}$). The maximum $ZT$ values (Figure 3) were obtained for a carrier concentration of 2 × $10^{20}$ and 7 × $10^{18}$ $cm^{-3}$ for p- and n-type conduction, respectively. At these carrier concentrations, the maximum Seebeck coefficient and power factor obtained for n-type conduction are 154.8 $\mu V\ K^{-1}$ and 2.7 $mW\ m^{-1}\ K^{-2}$, and those for p-type are 235.6 $\mu V\ K^{-1}$ and 10.8 $mW\ m^{-1}\ K^{-2}$, respectively. The lower value of the Seebeck coefficient for n-type conduction can be attributed to highly dispersive conduction bands leading to a very low effective mass (~0.05$m_e$). As expected, an exceptionally high $ZT$ value of ~2.21 was obtained for p-type as compared to that of 0.76 for n-type conduction.

Because of the quasi-2D nature, KMgBi has anisotropic transport properties. Figure 3c,k and Figure 3d,l show the variation of in-plane and out-of-plane Seebeck coefficients and power factors for p-type and n-type conductions with the logarithm of the carrier concentration log($n$). These values are shown at 600 K for p-type and 900 K for n-type conduction, which are the temperatures corresponding to their respective $ZT_{max}$. It can be seen that the in-plane power factor is very high as compared to the out-of-plane value for p-type conduction. This is due to the smaller values of $\sigma$ in the out-of-plane direction. The relatively higher value of $S$ along the out-of-plane direction for p-type conduction (valence bands from Γ−$Z$) is due to the much higher value of the effective mass (~6.14$m_e$). However, the anisotropy in $S$ is weak for n-type conduction. Figure 3g,o and Figure 3h,p show the variation of in-plane and out-of-plane total thermal conductivities and $ZT$ for p-type and n-type conductions with carrier concentration ($n$). There is high anisotropy in $\kappa$ values for p-type conduction as compared to that for n-type conduction. It can be seen that, for p-type conduction, the in-plane $ZT$ value is quite high


https://doi.org/10.1021/acsaem.2c01685
ACS Appl. Energy Mater. 2022, 5, 9141−9148

(~2.32), whereas for the n-type conduction, the out-of-plane ZT value is high (~1.25).

**Enhancing TE Performance via Alloy Engineering.** Thermoelectric properties of a given material are quite sensitive to its band gap (along with the curvature at/near the band edges). Although a small band gap allows easy excitation of electrons across the band edges, it concurrently compromises the Seebeck coefficient because of the increase in charge carrier concentration. Figure 4a shows the calculated *T*-

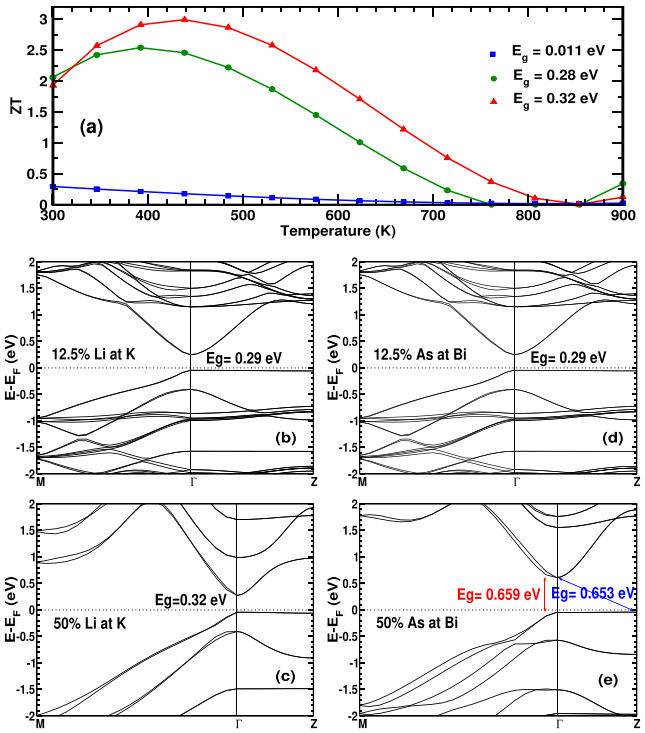


**Figure 4.** (a) Temperature dependence of *ZT* at optimal carrier concentrations for p-type conduction of KMgBi using three different band gap values (i.e., 0.011, 0.28, and 0.32 eV). The optimal carrier concentrations for the three cases are $1 \times 10^{20}$, $1 \times 10^{20}$, and $9 \times 10^{19}$ $cm^{-3}$, respectively. The HSE06+SOC band structure of alloyed KMgBi for (b) 12.5% Li at K sites, (c) 50% Li at K sites, (d)12.5% As at Bi sites, and (e) 50% As at Bi sites.

dependence of *ZT* for p-type conduction of KMgBi using three different band gap values, keeping the band curvature unchanged. The plot clearly indicates that *ZT* can increase if we can somehow enhance the band gap of KMgBi, keeping the changes in band topology minimal. This motivates us to explore a few selected alloys that can increase the band gap of KMgBi, keeping the flat valence band character along the Γ−*Z* intact. As evident from Figure 2a, the valence band edges are dominated by Bi states, whereas conduction band edges have contributions from all three atoms. From our previous studies on KMgBi and LiBiMg, the latter is known to have a larger band gap in the cubic phase.[25] Also, substituting heavier elements at K sites (like Rb, Cs) in its stable tetragonal phase is known to decrease the band gap.[27] This suggests the exploration of Li mixing at K sites. Also, as evident from Figure SIII of the Supporting Information,[41] SOC effects due to Bi heavily reduces the band gap. Thus, a suitable alloy (e.g., an isovalent lighter element) at Bi sites might help to increase the band gap. This tells us to explore As as a possible substitution at Bi sites. The band structures and atom projected density of states for various alloyed configurations are shown in Figure 4b−e and Figure SVIII of the Supporting Information, respectively.

*Alloying Li at K Sites.* Two different alloying concentrations (12.5% and 50%) were tried for Li at K sites. Figures SIV and SV of the Supporting Information[41] show the band structures of these alloys within (a) PBE, (b) PBE+SOC, (c) HSE06, and (d) HSE06+SOC functionals. For 12.5% Li at K sites, a direct band gap of 0.39 eV is observed at the PBE level, which closes when SOC is taken into account. With HSE06, however, a direct band gap of 0.88 eV is observed, which reduces to 0.29 eV with the inclusion of SOC. Note that, in all the calculations, enhancement in the band gap is observed as compared to the undoped KMgBi case. Similarly, 50% Li at K sites also shows enhancement in the band gap values, as expected. A close inspection of Figure SIII indicates that the nature of the band gap is indirect (0.31 eV) at the PBE level because of the rise of valence bands along the Γ to *X* direction. This feature, however, disappears when SOC is taken into account. Such an uphill of certain valence bands makes the band flatter, which is again a favorable feature for better TE performance. HSE06+SOC band structures for the two alloys are also presented in Figure 4b,c. Most interestingly, the band curvature including the flat valence band feature (near $E_F$) in both alloys almost remains unchanged as compared to that of pure KMgBi. There are, of course, some band splitting and/or an increased number of bands resulting from the larger size of the unit cell.

*Alloying As at Bi Sites.* As discussed earlier, because of the presence of Bi (heavy atom), spin−orbit effects are more evident in KMgBi. It is this effect that is primarily responsible for the decrease in the band gap at the HSE06 level, or the closure of the gap at the PBE level. One of the ways to reduce these effects is to substitute a lighter, isovalent element at the Bi site. Two different alloying concentrations (12.5% and 50%) were tried with As substitution at the Bi sites. Figures SVI and SVII of the Supporting Information[41] show the band structure of these alloys at the level of (a) PBE, (b) PBE+SOC, (c) HSE06, and (d) HSE06+SOC exchange-correlation functionals. The HSE06+SOC band structures for these alloys are also shown in Figure 4d,e. With 12.5% As alloying at Bi sites, the band gap increases from 0.83 eV (pure KMgBi) to 0.9 eV at the HSE06 level and from 0.22 eV (pure KMgBi) to 0.29 eV at the HSE06+SOC level. Unlike PBE+SOC, which closes the band gap, HSE06+SOC still keeps it semiconducting with a band gap value of 0.29 eV.

For 50% As alloying at Bi sites, interestingly a band gap of 0.14 eV is obtained, even within PBE+SOC, in contrast to all previous cases. HSE06+SOC predicts the most accurate band gap, which in this case is ~0.65 eV. A negligible difference between the direct and indirect band gap is observed for all band structures. As before, the flat band feature of the valence band edges still remains intact after alloying, which is beneficial for achieving enhanced TE properties. A comparison of the density of states of the various dopant configurations with pure KMgBi is shown in Supporting Information. This increase in band gap with alloying can be viewed as shifting of conduction (valence) bands to higher (lower) energies, without much effect on the overall band curvature. As such, an enhancement in the TE properties is expected with the above-specified alloying.


https://doi.org/10.1021/acsaem.2c01685
ACS Appl. Energy Mater. 2022, 5, 9141−9148

## CONCLUSION

We have theoretically investigated the unexplored thermoelectric properties of the experimentally synthesized KMgBi. A detailed electronic structure, phonon, and thermoelectric properties were simulated and a quasi-2D nature of this material has been established from both electron and phonon band structure. Unlike most other ab initio calculations, we have performed a more accurate prediction of band gap ($E_g$) and band order using the hybrid HSE06+GW approach. From the band topology, we predict topological trivial nature of this compound. Such accurate estimate of $E_g$ is also highly desired for the reliable prediction of thermoelectric properties. SOC is found to play an important role because of the heavier element Bi. The inclusion of SOC maintains the flat band feature of the valence band edges. Such flat bands are quite advantageous for promising electron transport. KMgBi also shows excellent thermal transport, including a low value of lattice thermal conductivity. This arises because of the high degree of anharmonicity. Such favorable electronic and thermal transport makes KMgBi a promising candidate (with a TE figure of merit $ZT$ as high as 2.21). For further enhancement of the TE efficiency, various substitutional alloying in KMgBi is explored. This helps to enhance the band gap, maintaining the flat band nature of the valence band edges intact. It is found that Li, being the lighter element, helps to increase the band gap when alloyed with potassium (K). Also, arsenic doping at Bi sites reduces the spin−orbit coupling, thereby again increasing the band gap. With the proposed alloying, we expect a 10−11% increase in $ZT$ for KMgBi. The ultralow $\kappa_L$ and high $ZT$ values make KMgBi an extremely promising TE candidate for future experimental exploration.

## ASSOCIATED CONTENT

### Supporting Information

The Supporting Information is available free of charge at https://pubs.acs.org/doi/10.1021/acsaem.2c01685.

(I) Computational methods, (II) electronic structure and density of states, (III) phonon dispersion and density of states, (IV) topological behavior, and (VI) carrier relaxation time (PDF)

## AUTHOR INFORMATION


### Corresponding Author

**Aftab Alam** − *Department of Physics, Indian Institute of Technology Bombay, Mumbai 400 076, India;* orcid.org/0000-0001-8458-1006; Email: aftab@iitb.ac.in

### Authors

**Vikram** − *Department of Chemistry, University of Reading Whiteknights, Reading, Berkshire RG6 6AD, United Kingdom*

**Bhawna Sahni** − *Department of Physics, Indian Institute of Technology Bombay, Mumbai 400 076, India*

**Ankit Jain** − *Mechanical Engineering Department, Indian Institute of Technology Bombay, Mumbai 400 076, India;* orcid.org/0000-0001-8091-9129

Complete contact information is available at: https://pubs.acs.org/10.1021/acsaem.2c01685

### Author Contributions

§V. and B.S. contributed equally to this work.

### Notes

The authors declare no competing financial interest.


## ACKNOWLEDGMENTS

B.S. acknowledges the financial support from the Indian Institute of Technology, Bombay, in the form of a teaching assistantship. A.A. acknowledges DST-SERB (Grant No. CRG/2019/002050) for funding to support this research. A.J. acknowledges the financial support from the National Supercomputing Mission, Government of India (Grant No.: DST/NSM/R and D-HPC-Applications/2021/10) and Nano Mission, Government of India (Grant No.: DST/NM/NS/2020/340). The lattice thermal conductivity calculations are carried out on the PARAM Sanganak supercomputing facility of IIT Kanpur.

## REFERENCES


(1) Tritt, T. M. Thermoelectrics Run Hot and Cold. *Science* **1996**, *272*, 1276−1277.

(2) DiSalvo, F. J. Thermoelectric Cooling and Power Generation. *Science* **1999**, *285*, 703−706.

(3) Chung, D.-Y.; Hogan, T.; Brazis, P.; Rocci-Lane, M.; Kannewurf, C.; Bastea, M.; Uher, C.; Kanatzidis, M. G. $CsBi_4Te_6$: A high-performance thermoelectric material for low- temperature applications. *Science* **2000**, *287*, 1024−1027.

(4) Littleton, R. T., IV; Tritt, T. M.; Kolis, J. W.; Ketchum, D. R. Transition-metal pentatellurides as potential low-temperature thermoelectric refrigeration materials. *Phys. Rev. B* **1999**, *60*, 13453.

(5) Nolas, G. S.; Kaeser, M.; Littleton, R. T., IV; Tritt, T. M. High figure of merit in partially filled ytterbium skutterudite materials. *Appl. Phys. Lett.* **2000**, *77*, 1855.

(6) Sales, B. C.; Mandrus, D.; Williams, R. K. Filled skutterudite antimonides: A new class of thermoelectric materials. *Science* **1996**, *272*, 1325.

(7) Gutierrez Moreno, J. J.; Cao, J.; Fronzi, M.; Assadi, M. H. N. A review of recent progress in thermoelectric materials through computational methods. *Materials for Renewable and Sustainable Energy* **2020**, *9*, 16.

(8) Huang, L.; Zhang, Q.; Yuan, B.; Lai, X.; Yan, X.; Ren, Z. Recent progress in half-Heusler thermoelectric materials. *Mater. Res. Bull.* **2016**, *76*, 107.

(9) Pope, A. L.; Tritt, T. M.; Chernikov, M. A.; Feuerbacher, M. Thermal and electrical transport properties of the single-phase quasicrystalline material:$Al_{70.8}Pd_{20.9}Mn_{8.3}$. *Appl. Phys. Lett.* **1999**, *75*, 1854.

(10) Shen, Q.; Chen, L.; Goto, T.; Hirai, T.; Yang, J.; Meisner, G. P.; Uher, C. Effects of partial substitution of Ni by Pd on the thermoelectric properties of ZrNiSn based half-Heusler compounds. *Appl. Phys. Lett.* **2001**, *79*, 4165.

(11) Sakurada, S.; Shutoh, N. Effect of Ti substitution on the thermoelectric properties of (Zr,Hf)NiSn half-Heusler compounds. *Appl. Phys. Lett.* **2005**, *86*, 082105.

(12) Yu, C.; Zhu, T. J.; Shi, R. Z.; Zhang, Y.; Zhao, X. B.; He, J. High-performance half-Heusler thermoelectric materials $Hf_{1-x}Zr_xNiSn_{1-y}Sb_y$ prepared by levitation melting and spark plasma sintering. *Acta Mater.* **2009**, *57*, 2757−2764.

(13) Liu, W. S.; Zhang, Q.; Lan, Y.; Chen, S.; Yan, X.; Zhang, Q.; Wang, H.; Wang, D.; Chen, G.; Ren, Z. Thermoelectric Property Studies on Cu-Doped n-type $Cu_xBi_2Te_{2.7}Se_{0.3}$ Nanocomposites. *Adv. Energy Mater.* **2011**, *1*, 577.

(14) Zhang, Q.; Cao, F.; Liu, W.; Lukas, K.; Yu, B.; Chen, S.; Opeil, C.; Broido, D.; Chen, G.; Ren, Z. Heavy Doping and Band Engineering by Potassium to Improve the Thermoelectric Figure of Merit in p-Type PbTe, PbSe, and $PbTe_{1-y}Se_y$. *J. Am. Chem. Soc.* **2012**, *134*, 10031.

(15) Jie, Q.; Wang, H.; Liu, W.; Wang, H.; Chen, G.; Ren, Z. Fast phase formation of double-filled p-type skutterudites by ball-milling and hot-pressing. *Phys. Chem. Chem. Phys.* **2013**, *15*, 6809.
(16) Yu, B.; Zebarjadi, M.; Wang, H.; Lukas, K.; Wang, H.; Wang, D.; Opeil, C.; Dresselhaus, M.; Chen, G.; Ren, Z. Enhancement of Thermoelectric Properties by Modulation-Doping in Silicon Germanium Alloy Nanocomposites. *Nano Lett.* **2012**, *12*, 2077.
(17) Kimura, Y.; Tamura, Y.; Kita, T. Thermoelectric properties of directionally solidified half-Heusler compound NbCoSn alloys. *Appl. Phys. Lett.* **2008**, *92*, 012105.
(18) Xia, Y.; Ponnambalam, V.; Bhattacharya, S.; Pope, A. L.; Poon, S. J.; Tritt, T. M. Electrical transport properties of TiCoSb half-Heusler phases that exhibit high resistivity. *J. Phys.: Condens. Matter* **2001**, *13*, 77.
(19) Kalarasse, F.; Bennecer, B. Structural and elastic properties of the filled tetrahedral semiconductors LiZnX (XZN, P, and As). *J. Phys. Chem. Solids* **2006**, *67*, 846−850.
(20) Mehnane, H.; Bekkouche, B.; Kacimi, S.; Hallouche, A.; Djermouni, M.; Zaoui, A. First-principles study of new half Heusler for optoelectronic applications. *Superlattices Microstruct.* **2012**, *51*, 772−784.
(21) Kacimi, S.; Mehnane, H.; Zaoui, A. I-II-V and I-III-IV half-Heusler compounds for optoelectronic applications: Comparative ab initio study. *J. Alloys Compd.* **2014**, *587*, 451−458.
(22) Roy, A.; Bennett, J. W.; Rabe, K. M.; Vanderbilt, D. Half-Heusler Semiconductors as Piezoelectrics. *Phys. Rev. Lett.* **2012**, *109*, 037602.
(23) Wang, X. T.; Dai, X. F.; Jia, H. Y.; Wang, L. Y.; Liu, X. F.; Cui, Y. T.; Liu, G. D. Topological insulating characteristic in half-Heusler compounds composed of light elements. *Phys. Lett. A* **2014**, *378*, 1662−1666.
(24) Arif, M.; Murtaza, G.; Ali, R.; Khenata, R.; Takagiwa, Y.; Muzammil, M.; Omran, S. B. Elastic and electro-optical properties of XYZ (X= Li, Na and K; Y= Mg; Z= N, P, As, Sb and Bi) compounds. *Indian Journal of Physics* **2016**, *90*, 639−647.
(25) Sahni, B.; Vikram; Kangsabanik, J.; Alam, A. Reliable Prediction of New Quantum Materials for Topological and Renewable-Energy Applications: A High-Throughput Screening. *J. Phys. Chem. Lett.* **2020**, *11*, 6364−6372.
(26) Bennett, J. W.; Garrity, K. F.; Rabe, K. M.; Vanderbilt, D. Hexagonal A B C semiconductors as ferroelectrics. *Physical review letters* **2012**, *109*, 167602.
(27) Le, C.; Qin, S.; Wu, X.; Dai, X.; Fu, P.; Fang, C.; Hu, J. Three-dimensional topological critical Dirac semimetal in AMgBi (A= K, Rb, Cs). *Phys. Rev. B* **2017**, *96*, 115121.
(28) Wieder, B. J.; Wang, Z.; Cano, J.; Dai, X.; Schoop, L. M.; Bradlyn, B.; Bernevig, B. A. Strong and fragile topological Dirac semimetals with higher-order Fermi arcs. *Nat. Commun.* **2020**, *11*, 627.
(29) Zhang, X.; Sun, S.; Lei, H. Narrow-gap semiconducting properties of KMgBi with multiband feature. *Phys. Rev. B* **2017**, *95*, 035209.
(30) Goyal, V.; Teweldebrhan, D.; Balandin, A. A. Mechanically-exfoliated stacks of thin films of $Bi_2Te_3$ topological insulators with enhanced thermoelectric performance. *Appl. Phys. Lett.* **2010**, *97*, 133117.
(31) Hossain, M. Z.; Rumyantsev, S. L.; Teweldebrhan, D.; Shahil, K. M. F.; Shur, M.; Balandin, A. A. 1/fnoise in conducting channels oftopological insulator materials. *Physica Status Solidi A* **2011**, *208*, 144−146.
(32) Hicks, L. D.; Dresselhaus, M. S. Effect of quantum-well structures on the thermoelectric figure of merit. *Phys. Rev. B* **1993**, *47*, 12727.
(33) Hohenberg, P.; Kohn, W. Inhomogeneous electron gas. *Phys. Rev.* **1964**, *136*, B864.
(34) Kresse, G.; Furthmüller, J. Efficiency of ab-initio total energy calculations for metals and semiconductors using a plane-wave basis set. *Comput. Mater. Sci.* **1996**, *6*, 15.
(35) Kresse, G.; Furthmüller, J. Efficient iterative schemes for ab initio total-energy calculations using a plane-wave basis set. *Phys. Rev. B* **1996**, *54*, 11169.
(36) Kresse, G.; Hafner, J. Ab initio molecular dynamics for liquid metals. *Phys. Rev. B* **1993**, *47*, 558.
(37) Blöchl, P. E. Projector augmented-wave method. *Phys. Rev. B* **1994**, *50*, 17953−17979.
(38) Perdew, J. P.; Burke, K.; Ernzerhof, M. Generalized gradient approximation made simple. *Phys. Rev. Lett.* **1996**, *77*, 3865.
(39) Krukau, A. V.; Vydrov, O. A.; Izmaylov, A. F.; Scuseria, G. E. Influence of the exchange screening parameter on the performance of screened hybrid functionals. *J. Chem. Phys.* **2006**, *125*, 224106.
(40) Aryasetiawan, F.; Gunnarsson, O. The GW method. *Rep. Prog. Phys.* **1998**, *61*, 237−312. Onida, G.; Reining, L.; Rubio, A. Electronic excitations: density-functional versus many-body Green's-function approaches. *Rev. Mod. Phys.* **2002**, *74*, 601−659. Perdew, J. P.; Burke, K.; Ernzerhof, M. Generalized Gradient Approximation Made Simple. *Phys. Rev. Lett.* **1996**, *77*, 3865−3868.
(41) See the Supporting Information. There, we provide further details on computational methods, electronic band structures and density of states, phonon band structures and density of states, and carrier relaxation times; we also include references.[43,44]
(42) Ganose, A. M.; Park, J.; Faghaninia, A.; Woods-Robinson, R.; Persson, K. A.; Jain, A. Efficient calculation of carrier scattering rates from first principles. *Nat. Commun.* **2021**, *12*, 2222.
(43) Morales-García, Á.; Valero, R.; Illas, F. An Empirical, yet Practical Way To Predict the Band Gap in Solids by Using Density Functional Band Structure Calculations. *J. Phys. Chem. C* **2017**, *121*, 18862−18866.
(44) Reissland, J. A. *The Physics of Phonons*; John Wiley and Sons Ltd.: 1973.
(45) Dove, M. T. *The Introduction to Lattice Dynamics*; Cambridge University Press: Cambridge, 1993.
(46) Jain, A. Multichannel thermal transport in crystalline $Tl_3VSe_4$. *Phys. Rev. B* **2020**, *102*, 201201.
(47) Yang, J.; Li, H.; Wu, T.; Zhang, W.; Chen, L.; Yang, J. Evaluation of Half-Heusler Compounds as Thermoelectric Materials based on the calculated electrical transport properties. *Adv. funct. Mater.* **2008**, *18*, 2880−2888.
(48) Chen, W.; Pohls, J.-H.; Hautier, G.; Broberg, D.; Bajaj, S.; Aydemir, U.; Gibbs, Z. M.; Zhu, H.; Asta, M.; Snyder, G. J.; Meredig, B.; White, M. A.; Persson, K.; Jain, A. Understanding thermoelectric properties from high-throughput calculations: trends, insights, and comparisons with experiment. *J. Mater. Chem. C* **2016**, *4*, 4414.
(49) Madsen, G. K.H.; Singh, D. J. BoltzTrap. A code for calculating band-structure dependent quantities. *Comput. Phys. Commun.* **2006**, *175*, 67.
(50) Gong, J. J.; Hong, A. J.; Shuai, J.; Li, L.; Yan, Z. B.; Ren, Z. F.; Liu, J.-M. Investigation of the bipolar effect in the thermoelectric material $CaMg_2Bi_2$ using a first principles study. *Phys. Chem. Chem. Phys.* **2016**, *18*, 16566.


https://doi.org/10.1021/acsaem.2c01685
ACS Appl. Energy Mater. 2022, 5, 9141−9148